Int. J. Adv. Appl. Math. and Mech. 12(1) (2024) 57 – 69 (ISSN: 2347-2529)

Journal homepage: www.ijaamm.com

IJAAMM

International Journal of Advances in Applied Mathematics and Mechanics

Heat Transfer on a Non-Newtonian Hydromagnetic Fluid Flow through a Convergent Conduit with Chemical Reaction and Soret Effects

Research Article

Njue Caroline Wawira*, Edward Richard Onyango, David Chepkonga

Department of Pure and Applied Mathematics, Jomo Kenyatta University of Agriculture and Technology, Juja, 62000-00200, Nairobi, Kenya

Received 16 August 2024; accepted (in revised version) 13 September 2024

Abstract: In this study, the chemical reaction and Soret effects of an unsteady, incompressible, non-Newtonian fluid flow through a convergent conduit taking into account joule heating, viscous dissipation, variable magnetic field, heat and mass transfer has been considered. The flow problem is mathematically modeled, where the governing non-linear partial differential equations are transformed into ordinary differential equations. The resulting dimensionless ordinary differential equations are solved numerically using the collocation method and simulated in MATLAB software to obtain the flow profiles and the effect of flow parameters on the flow variables. The simulation results are presented graphically and in tabular form. The results showed that concentration decreases with an increase in the chemical reaction parameter, Soret parameter and the Schimdt number. Further, the Nusselt number increases with an increase in the Eckerts number. The results are significant and the insight obtained in the study can be applied in areas such as; extraction of molten polymer flows through convergent dies and fluid flow through the convergent conduit subsequent to the Pelton turbine. Thus the fluid velocity can be increased by reducing the radius of the conduit and providing appropriate insulators at the wall to minimize heat loss at the conduit's wall.

MSC: 80Axx • 92Bxx

Keywords: Soret effects • Chemical reactions • Variable magnetic field • Convergent conduit

1. Introduction

In recent years, numerous research has been done on fluid flow through convergent conduit due to its wide applications in industrial and various engineering disciplines. Some of the applications include the fluid flow through convergent conduit subsequent to the water turbines, in hybrid rocket engines where the fluid flowing through the convergent nozzle/conduit is utilized to control the exhaust flow and produce thrust and in extrusion of molten polymer through convergent dies.

For instance in sheet or film extrusion, the molten polymer flows through the convergent dies to reduce the thickness of the extruded material. The converging dies are basically used to control the thickness of the final film or sheet by ensuring the polymer chains orient and align in the direction of flow. The study on fluid flowing through convergent/ divergent conduit was first initiated by [1] and [2].

[3] investigated the effect of thermal radiation on a two-dimensional, incompressible, Newtonian fluid flow through stretchable convergent/divergent channels under a constant magnetic field. The system of non-linear partial differential equations governing the flow was transformed into ordinary differential equations and solved analytically by

* Corresponding author.

E-mail address(es): wawira.caroline2021@students.jkuat.ac.ke (Njue Caroline Wawira), edward.onyango@jkuat.ac.ke (Edward Richard Onyango), chepkongadavid@gmail.com (David Chepkonga).

Nomenclature

		(Units)
B	Magnetic flux	wbm^{-2}
E	Electric Field Intensity	Vm^{-1}
H_r, H_θ	Induced Magnetic Field in r and θ direction respectively,	Am^{-1}
F_e	Electromagnetic force	N
C_p	Specific heat capacity	$Jkg^{-1}K^{-1}$
C_f	Skin Friction Coefficient	
t	Time	s
r	Characteristic radius	m
ρ	Fluid density	Kg/m^3
m	Arbitrary constant related to conduit's angle	
K_T	Thermal Diffusivity ratio, $\frac{k}{\rho C_p}$	
k	Thermal conductivity	$Wm^{-1}k^{-1}$
D_m	Mass diffusivity	
T_m	Mean fluid temperature	K
δ	Time dependent length scale	
μ_o	Dynamic viscosity	$kgm^{-1}s^{-1}$
ν	Kinematic Viscosity	m/s^2
σ	Electrical conductivity	$\Omega^{-1}m^{-1}$
β	Friction coefficient factor	
η	Magnetic diffusivity	m^2/s
μ_e	Magnetic permeability	Hm^{-1}
ϵ	Electrical Permittivity	$C^2N^{-1}m^{-2}$
α	Conduit's semi angle	$Radian$
F	Dimensionless Velocity	
ω	Dimensionless Temperature	
φ	Dimensionless induced magnetic field in θ direction	
γ	Dimensionless induced magnetic field in r direction	
ϕ	Dimensionless Concentration	

employing Adomian's decomposition method. The results showed that temperature decreased as the radiation number increased and the heat transfer at the walls decreased due to differences in radiation number for both convergent and divergent channels.

Nagler [4], studied an incompressible, two-dimensional, unsteady, non-Newtonian fluid flow through a convergent conduit taking into account the wall friction and neglecting the body forces. The resulting Partial Differential Equations governing the flow were solved numerically by the collocation method. In the study, the viscosity was considered as a function of the tangential direction. He discovered that the fluid velocity reduces gradually with an increase in the tangential direction. Further, the results showed that an increase in the friction coefficient led to a decrease in velocity values but an increase in the Reynolds number increased the velocity profiles.

[5] studied the Soret effects and chemical reaction in a free convectional flow past a vertical porous plate in the presence of a constant magnetic field. The study considered a steady, incompressible, laminar flow neglecting the viscous dissipation and induced magnetic field. The governing partial differential equations were solved numerically. The results showed that the concentration increases with the increase of the Prandtl number and heat source parameter. Further, the concentration decreases with the increase of chemical reaction parameter and the Schmidt number (Sc) increases with the decrease of concentration.

[6], studied the heat and mass transfer of an incompressible Newtonian fluid flow taking into account the effect of thermal diffusion in vertical porous plates. The study neglected the induced magnetic field and the governing equations were solved analytically using the adopting perturbation technique. The results showed that the fluid velocity decreased with an increase in the magnetic parameter but increased with an increase in the Soret number. Further, the concentration in the fluid increases with increasing values of the Soret number and decreases with an increase in the Schmdit number.

In the study [7], an unsteady, incompressible Jeffrey-Hamel flow in the presence of an inclined variable magnetic field with heat and mass transfer was investigated. The equations governing the flow were solved numerically using the collocation method. As per the results, the temperature increases with the increase in the Eckert number, Grashof Temperature number, Hartmann number, wedge angle, and the Prandtl number. Further, the concentration of the fluid increases with the increase in the unsteadiness parameter and the wedge angle parameter while it decreases with the increase in the Reynolds number.

[8] studied a two-dimensional, incompressible, electrically conducting nanofluid through a convergent/divergent

conduit with porous media. The study took into account constant magnetic field and the governing Naiver Stokes equations were solved using the Homotopy perturbation method. The results showed that an increase in the conduit's angle along the flow reduced the fluid flow. Consequently, the temperature reduced with an increase in the Darcy number.

[9] examined the heat and mass transfer of an unsteady MHD flow of a viscous, incompressible and electrically conducting fluid past a porous plate accounting for viscous dissipation, chemical reaction and heat generations. The governing equations are solved numerically using the crank-Nicolson finite difference method. The results show that the velocity, temperature and concentration profiles increased as time increased. Further, the velocity and concentration profiles decrease as the Chemical reaction parameter increases.

Wawira [10], examined an unsteady, non-Newtonian (dilatant) fluid flow through a convergent conduit in the presence of variable magnetic field, Joule heating, viscous dissipation and skin friction. The partial differential equations governing the flow were transformed into ordinary differential equations and solved numerically using the collocation method. The results indicated that an increase in the Eckert's number, Reynolds number and the Joule heating parameter increases the fluid's velocity, while an increase in the Hartmann number and the unsteadiness parameter decreases the convective heat transfer and the fluid's velocity. Further, the skin friction coefficient decreases with an increase in the Reynolds number, the Hartmann number, and the Joule heating parameter.

Liberty, [11] studied a steady, two-dimensional hydromagnetic convective flow driven by a vertical porous plate under the influence of chemical reaction and radiation absorption in the presence of inclined magnetic field. The governing non-linear differential equations were solved analytically using the Temimi-Ansari method. The results depict that the Casson parameter and Grashof number positively correlated with the velocity gradient. In contrast, an increase in the Eckerts number, Magnetic parameter and heat source parameter enhanced the temperature distribution. Further, an increase in the Prandtl number reduced the temperature while the concentration decreased with an increase in Schmidt and Chemical reaction parameter.

However, in fluid flow through the convergent conduit, the presence of internal resistance, viscous dissipation and Joule heating creates a temperature gradient which leads to a mass flux in the flow (Soret effect). Additionally, the fluid flow provides a dynamic environment that can facilitate the occurrence of chemical reactions. Further, the interaction of the present magnetic field and the fluid's velocity induces an electric current which in turn induces magnetic field in the flow. This leads to a variable magnetic field i.e. the applied magnetic field plus the induced magnetic field in the flow.

Therefore, in light of the prior studies on fluid flow through convergent conduits, the Soret effect and chemical reactions on a non-Newtonian fluid flow through a convergent conduit in the presence of viscous dissipation, Joule heating and variable magnetic field have been neglected. However, in real-life problems, the existence of a temperature difference in a fluid flow creates a species concentration gradient (mass flux) in the flow which alters the fluid velocity in the convergent conduit. Similarly, the chemical reactions in the flow affect the flow profiles.

Hence motivated by prior studies, the study provides a comprehensive insight into the heat and mass transfer of a non-Newtonian fluid flow accounting for the existing Soret effects, chemical reaction, viscous dissipation, Joule heating, skin friction and variable magnetic field. This is done by formulating the mathematical model for the flow problem, numerically solving the governing partial differential equations by the collocation method and presenting the obtained results graphically and on a data table.

2. Mathematical Formulation

The present study considers an unsteady, incompressible, two-dimensional, non-Newtonian hydromagnetic fluid flow through a convergent conduit restricted to the laminar domain. The fluid exhibits a constant thermal and electrical conductivity while the conduit's wall is electrically non-conducting. The flow through the convergent conduit is described using the cylindrical coordinate system (r,θ,z) where r,θ and z represent the radial, tangential and axial directions respectively. The fluid flow is purely radial and the flow field is infinite in the z direction. A variable magnetic field has been considered where a magnetic field is applied in the tangential direction and the induced magnetic field in r and θ directions are taken into account hence the total magnetic field $\mathbf{B} = \mu_e H_r \mathbf{r} + \mu_e (H_\theta^* + H_\theta)$. Further, viscous dissipation, joule heating, skin friction, the Soret effect, chemical reactions and the rate of heat & mass transfer are taken into account. In the context of our study, $T_\infty > T_w$, where T_∞ and T_w are the free stream and wall temperature respectively. Further, the $C_\infty < C_w$ where C_∞ and C_w are the free stream and wall concentration respectively. In the study, there is no particle slip at the conduit's wall hence the no-slip boundary condition is applied. This implies that the fluid velocity at the wall assumes zero velocity relative to the wall surface. Further, the force due to induced electric field $\rho\mathbf{E}$ is negligible compared to the Lorentz force $\mathbf{F} = \mathbf{J} \times \mathbf{B}$ due to the magnetic field.

The flow configuration is shown in Fig. 1,

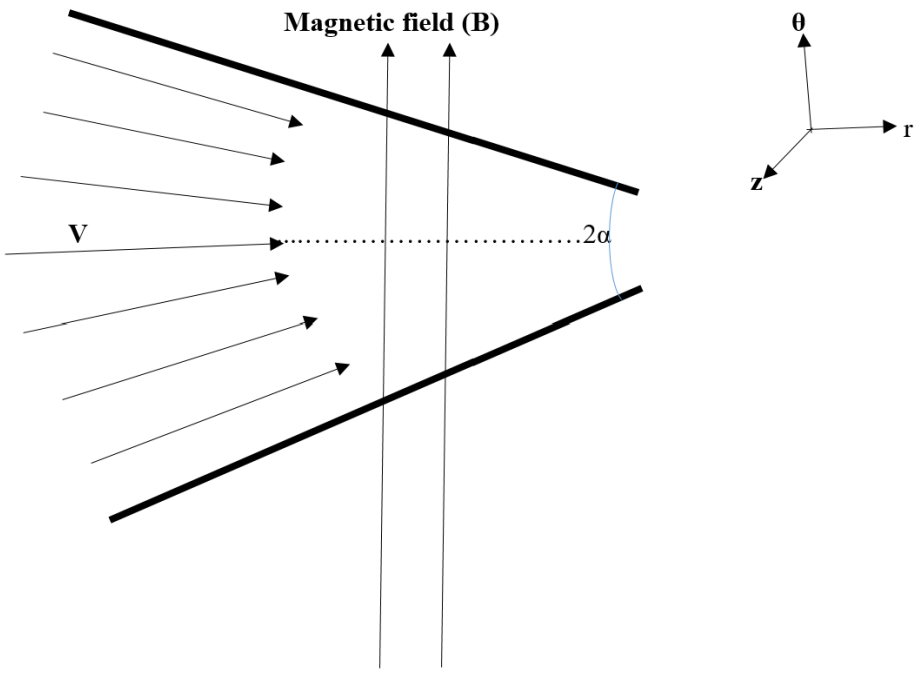

Fig. 1. Schematic Flow Configuration

2.1. The Governing Equations

The system of equations governing the flow taking into account the respective assumptions of the study includes the continuity, momentum, energy, magnetic induction and concentration equations. These equations are represented as follows;

Continuity Equation

$$\frac{\partial(rU_r)}{\partial r} = 0 \tag{1}$$

Momentum Equation

$$\begin{aligned}
&\frac{\partial^2 U_r}{\partial\theta\partial t} = \frac{2}{\rho}\frac{\partial U_r}{\partial r}\frac{\partial^2\mu}{\partial\theta\partial r} + \frac{2}{\rho}\frac{\partial\mu}{\partial r}\frac{\partial^2 U_r}{\partial\theta\partial r} + \frac{1}{\rho r^2}\frac{\partial U_r}{\partial\theta}\frac{\partial^2\mu}{\partial\theta^2} \\
&+ \frac{\partial\mu}{\partial\theta}\left(\frac{2}{\rho r^2}\frac{\partial^2 U_r}{\partial\theta^2} + \frac{2U_r}{\rho r^2} - \frac{2}{\rho r^2}\frac{\partial U_r}{\partial r}\right) + \frac{\mu}{\rho}\left(\frac{1}{r^2}\frac{\partial^3 U_r}{\partial\theta^3} - \frac{2}{r}\frac{\partial^2 U_r}{\partial r\partial\theta} + \frac{2}{r^2}\frac{\partial U_r}{\partial\theta}\right) - U_r\frac{\partial^2 U_r}{\partial\theta\partial r} \\
&- \frac{\partial U_r}{\partial r}\frac{\partial U_r}{\partial\theta} - \frac{1}{\rho}\frac{\partial U_r}{\partial\theta}\frac{\partial^2\mu}{\partial r^2} - \frac{1}{\rho}\frac{\partial\mu}{\partial r}\frac{\partial^2 U_r}{\partial r\partial\theta} - \frac{2}{\rho r}\frac{\partial U_r}{\partial\theta}\frac{\partial\mu}{\partial r} \\
&- \frac{2U_r}{\rho r}\frac{\partial^2\mu}{\partial r\partial\theta} - \frac{\sigma\mu_e^2(H_\theta^* + H_\theta)^2}{\rho}\frac{\partial U_r}{\partial\theta} - \frac{2\sigma U_r\mu_e^2(H_\theta^* + H_\theta)}{\rho}\frac{\partial H_\theta}{\partial\theta} \\
&- \frac{\sigma r\mu_e^2 H_\theta^* H_r}{\rho}\frac{\partial U_r}{\partial r} - \frac{\sigma U_r\mu_e^2 H_\theta^* H_r}{\rho} - \frac{\sigma r U_r\mu_e^2 H_\theta^*}{\rho}\frac{\partial H_r}{\partial r} - \frac{\sigma r U_r\mu_e^2 H_r}{\rho}\frac{\partial H_\theta}{\partial r} \\
&- \frac{\sigma r U_r\mu_e^2 H_\theta}{\rho}\frac{\partial H_r}{\partial r} - \frac{\sigma U_r\mu_e^2 H_\theta H_r}{\rho} - \frac{\sigma r\mu_e^2 H_r H_\theta}{\rho}\frac{\partial U_r}{\partial r}
\end{aligned} \tag{2}$$

Energy Equation

$$\begin{aligned}
&\frac{\partial T}{\partial t} = \frac{k}{\rho C_p}\left[\frac{1}{r}\frac{\partial T}{\partial r} + \frac{\partial^2 T}{\partial r^2} + \frac{1}{r^2}\frac{\partial^2 T}{\partial\theta^2}\right] + \frac{2\mu_o g^{n-1}}{\rho C_p}\left[(\frac{\partial U_r}{\partial r})^2 + (\frac{U_r}{r})^2\right] \\
&+ \frac{\mu_o g^{n-1}}{\rho C_p}\left[(\frac{1}{r}\frac{\partial U_r}{\partial\theta})^2\right] - U_r\frac{\partial T}{\partial r} + \frac{\sigma\mu_e^2 U_r^2 H_\theta^{*2}}{\rho C_p} + \frac{2\sigma\mu_e^2 U_r^2 H_\theta^* H_\theta}{\rho C_p} + \frac{\sigma\mu_e^2 U_r^2 H_\theta^2}{\rho C_p}
\end{aligned} \tag{3}$$

Magnetic Induction Equation in r direction

$$\frac{\partial H_r}{\partial t} = \frac{1}{\eta}\left[\frac{\partial^2 H_r}{\partial r^2} + \frac{1}{r}\frac{\partial H_r}{\partial r} + \frac{1}{r^2}\frac{\partial^2 H_r}{\partial \theta^2}\right] - \mu_e U_r \frac{\partial H_r}{\partial r} \tag{4}$$

Magnetic Induction Equation in θ direction

$$\frac{\partial H_\theta}{\partial t} = \frac{1}{\eta}\left[\frac{\partial^2 H_\theta}{\partial r^2} + \frac{1}{r}\frac{\partial H_\theta}{\partial r} + \frac{1}{r^2}\frac{\partial^2 H_\theta}{\partial \theta^2}\right] - \mu_e U_r \frac{\partial H_\theta}{\partial r} \tag{5}$$

Concentration Equation

$$\frac{\partial C}{\partial t} + U_r\frac{\partial C}{\partial r} = D_m\left[\frac{1}{r}\frac{\partial}{\partial r}(r\frac{\partial C}{\partial r}) + \frac{1}{r^2}\frac{\partial^2 C}{\partial \theta^2}\right] - K_r(C - C_\infty) + \frac{D_m K_T}{T_m}\frac{\partial^2 T}{\partial \theta^2} \tag{6}$$

The momentum equation 2 incorporates the Lorentz force taking into account both the applied and induced magnetic field in r and θ directions. Viscous dissipation and Joule heating have been incorporated in the energy equation 3. Further, the species/solute concentration equation 6 incorporates the source term related to first-order chemical reaction and mass flux resulting from the Soret effects.

The following boundary conditions have been considered as presented in various studies [7, 10, 12, 13].
At the centre line; at $\theta = 0$

$$U_r = U_\infty, \frac{\partial U_r}{\partial \theta} = 0, T = T_\infty, \frac{\partial T}{\partial \theta} = 0, C = C_\infty, \frac{\partial C}{\partial \theta} = 0 \tag{7}$$

At the Conduit's Wall; at $\theta = \alpha$

$$\frac{\partial U_r}{\partial \theta} = -\beta F(\theta), T = T_w, C = C_w \tag{8}$$

The system of nonlinear partial differential equations 2, 3, 4,5 and 6 are transformed into ordinary differential equations to facilitate the non-dimensionalization process. The transformation ensures that the number of variables in the flow problem is reduced and the obtained results apply to similar geometrical configurations under the same conditions. Furthermore, the transformation process leads to a systematic arrangement of variables, which form non-dimensional parameters that can be used to make logical deduction about the flow problem.

The following similarity transformations for velocity, the induced magnetic field in r and θ directions, temperature, concentration and viscosity are used as presented in [7], [10] and [22].

$$\begin{gathered} U_r(\theta,t) = -\frac{Q}{r}\frac{1}{\delta^{m+1}}F(\theta), \quad H_r(\theta,t) = -\frac{Q}{r}\frac{1}{\delta^{m+1}}\gamma(\theta), \quad H_\theta = -\frac{Q}{r}\frac{1}{\delta^{m+1}}\varphi(\theta) \\ \frac{\phi(\theta)}{\delta^{m+1}} = \frac{C - C_w}{C_\infty - C_w}, \quad \frac{\omega(\theta)}{\delta^{m+1}} = \frac{T - T_w}{T_\infty - T_w}, \quad \mu = \mu_o\theta^{c(n-1)}(\theta) \end{gathered} \tag{9}$$

Therefore, the final set of the dimensionless ordinary differential equations governing the flow problem is as follows;

$$\begin{gathered} c(n-1)\theta^{c(n-1)-2}\left[c(n-1)-1\right]F' + c(n-1)\theta^{c(n-1)-1}\left[2F'' + 4F\right] + \theta^{c(n-1)} \\ \left[F''' + 4F'\right] - 2R_e\frac{r}{\delta^{m+1}}FF' - Ha^2F' + R_m\frac{Ha}{r\sqrt{\sigma\mu_o}}\frac{1}{\delta^{m+1}}\left[2\varphi F' + 2F\varphi - \gamma F\right] \\ -Re.R_m\frac{r^2\mu_e}{\rho}\frac{1}{\delta^{2m+2}}\left[\varphi^2F' + 2F\varphi\varphi' - 2\gamma\varphi F\right] + (m+1)\frac{r^{m+1}}{\delta^{m+1}}\lambda F' = 0 \end{gathered} \tag{10}$$

$$\begin{gathered} (m+1)\frac{r^{m+1}}{\delta^{m+1}}\lambda\omega + \frac{1}{Pr}\omega'' + \theta^{c(n-1)}\frac{Ec}{\delta^{m+1}}\left[4F^2 + F'^2\right] \\ + \frac{J}{\delta^{m+1}}F^2 - 2r\sqrt{\frac{\mu_e}{\rho}\frac{ReR_m}{Ha^2}}\frac{J}{\delta^{2m+2}}F^2\varphi + \frac{r^2\mu_e}{\rho}\frac{ReR_m}{Ha^2}\frac{J}{\delta^{3m+3}}F^2\varphi^2 = 0 \end{gathered} \tag{11}$$

$$(m+1)\frac{r^{m-2}}{\delta^{2m+2}}\lambda\gamma + \frac{1}{Pr_{(m)}}\frac{1}{r^3}\frac{1}{\delta^{m+1}}\left[\gamma + \gamma''\right] - Re\frac{\mu_e}{r^2}\frac{1}{\delta^{2m+2}}F\gamma = 0 \tag{12}$$

$$(m+1)\frac{r^{m+1}}{\delta^{2m+2}}\lambda\varphi + \frac{1}{Pr_{(m)}}\frac{1}{\delta^{m+1}}\left[\varphi + \varphi''\right] - Re\mu_e\frac{r}{\delta^{2m+2}}F\varphi = 0 \tag{13}$$

$$(m+1)\frac{r^{m+1}}{\delta^{m+1}}\lambda\phi+\frac{1}{Sc}\phi''-r^2Sr\omega''-CrRe^2\phi=0 \tag{14}$$

Where the dimensionless parameters appearing in the above equations are defined as follows;
Reynolds number $R_e=\frac{Q\rho}{r\mu_o}$, magnetic Reynolds number $R_m=\mu_e\sigma\frac{Q}{r}$, the unsteadiness parameter $\lambda=\frac{\rho\delta^m}{\mu_o r^{m-1}}\frac{d\delta}{dt}$, Prandtl number $Pr=\frac{\mu_o}{\rho\alpha}$ where $\alpha=\frac{k}{\rho C_p}$, Eckert number $Ec=\frac{Q^2}{r^2}\frac{1}{C_p(T_\infty-T_w)}$, Hartmann number $Ha=B_o r(\frac{\sigma}{\mu_o})^{\frac{1}{2}}$, Joule heating parameter $J=\frac{\sigma\mu_e^2H^{*2}_\theta Q^2}{\mu_o C_p(T_\infty-T_w)}$, magnetic Prandtl number $Pr_{(m)}=\frac{\mu_e\sigma\mu_o}{\rho}$, Schmidt number $Sc=\frac{\mu_o}{\rho D_m}$, Chemical reaction Parameter $Cr=\frac{\mu_o K_r}{\rho U_r^2}$ and Soret number $Sr=\frac{\mu D_m K_T(T_w-T_\infty)}{\rho T_m(C_w-C_\infty)}$.

In the present study, the wedge angle parameter, skin friction coefficient, Sherwood number and the Nusselt number are parameters of practical interest. According to [7], [10] among other studies, these parameters can be expressed as follows; the wedge angle parameter expressed as $\Omega=2\alpha=\frac{2m}{m+1}\pi$, skin friction coefficient $C_f=\frac{2}{\sqrt{Re(2-\epsilon)}}F'(\theta)$ $Nu=-\sqrt{\frac{Re}{2-\epsilon}}\omega'(\theta)$, $Sh=-\sqrt{\frac{Re}{2-\epsilon}}\phi'(\theta)$, where $\epsilon=\frac{2m}{m+1}$.

Further, the similarity transformations in equation 9, are applied on the boundary conditions in equations 7 and 8 resulting to;

$$\begin{cases}\text{At the centre line;}\ \ \theta=0;\ \ F(0)=1,\ \ F'(0)=0,\ \ \omega(0)=\delta^{m+1},\ \ \phi(0)=0.\\ \text{On the conduits wall;}\ \ \theta=\alpha\ \ F'(\alpha)=-\beta F(\alpha),\ \ \omega(\alpha)=0,\ \ \phi(\alpha)=\delta^{m+1}.\end{cases} \tag{15}$$

2.2. Numerical Solution

The governing equations i.e the equation of motion, energy, magnetic induction in r & θ directions and concentration equations in the dimensionless form are essentially non-linear ordinary differential equations. Therefore, the collocation method is used to solve the system of equations 10 - 14 subject to the boundary conditions in equation 15. According to [25], the collocation method approximates the solution of boundary value problems (BVPs) in series form when the ODEs are of the form;

$$y'(\theta)=f(\theta,y(\theta));\qquad\qquad \theta\in[a,b] \tag{16}$$

The solution of the 2-point BVP in series form is given by;

$$y(\theta)=\sum_{j=1}^{n}C_jV_j(\theta)\qquad\qquad \theta\in[a,b] \tag{17}$$

where $C_1,C_2,C_3....C_n$ are unknown coefficients which are determined by imposing n collocation conditions in order to obtain an $n\times n$ system of linear equations. Therefore, considering that $\theta\in[0,\alpha]$, then the series form of equation 17 is;

$$\left.\begin{array}{c}\sum_{j=1}^{n}C_jV_j(0)=P\\ f(\theta_i)=\sum_{j=1}^{n}C_jV_j(\theta_i)\qquad i=2,3,4.....n-1\\ \sum_{j=1}^{n}C_jV_j(\alpha)=Q\end{array}\right\} \tag{18}$$

From equation 18, to obtain the $n-2$ equations, then $n-2$ collocation points $\theta_2,\theta_3,\theta_4,...,\theta_{n-1}$ are chosen and enforce in the differential equations. This yields a non-singular matrix.
The higher order ODEs 10 - 14 are reduced to a system of first-order ODEs using the definitions in equation 19.

$$y_1=F,\ y_2=F',\ y_3=F'',y_4=\omega,\ y_5=\omega',y_6=\gamma,\ \ y_7=\gamma',\ y_8=\varphi,\ y_9=\varphi',\ y_{10}=\phi,\ y_{11}=\phi' \tag{19}$$

Upon substituting the respective functions into equations 10 - 14 we obtained;

$$\begin{aligned}c(n-1)\theta^{c(n-1)-2}\left[c(n-1)-1\right]y_2+c(n-1)\theta^{c(n-1)-1}\left[2y_3+4y_1\right]\\ +\theta^{c(n-1)}\left[y'_3+4y_2\right]-2R_e\frac{r}{\delta^{m+1}}y_1y_2-Ha^2y_2\\ +R_m\frac{Ha}{r\sqrt{\sigma\mu_o}}\frac{1}{\delta^{m+1}}\left[2y_8y_2+2y_1y_8-y_6y_1\right]\\ -Re.R_m\frac{r^2\mu_e}{\rho}\frac{1}{\delta^{2m+2}}\left[y_8^2y_2+2y_1y_8y_9-2y_6y_8y_1\right]+(m+1)\frac{r^{m+1}}{\delta^{m+1}}\lambda y_2=0\end{aligned} \tag{20}$$

$$(m+1)\frac{r^{m+1}}{\delta^{m+1}}\lambda y_4+\frac{1}{Pr}y_5^{'}+\theta^{c(n-1)}\frac{Ec}{\delta^{m+1}}\left[4y_1^2+y_2^2\right]$$
$$+\frac{J}{\delta^{m+1}}y_1^2-2r\sqrt{\frac{\mu_e}{\rho}\frac{ReR_m}{Ha^2}}\frac{J}{\delta^{2m+2}}y_1^2y_8+\frac{r^2\mu_e}{\rho}\frac{ReR_m}{Ha^2}\frac{J}{\delta^{3m+3}}y_1^2y_8^2=0 \tag{21}$$

$$(m+1)\frac{r^{m+1}}{\delta^{2m+2}}\lambda y_6+\frac{1}{Pr_{(m)}}\frac{1}{\delta^{m+1}}\left[y_6+y_7^{'}\right]-Re\mu_e\frac{r}{\delta^{2m+m}}y_1y_6=0 \tag{22}$$

$$(m+1)\frac{r^{m+1}}{\delta^{2m+2}}\lambda y_8+\frac{1}{Pr_{(m)}}\frac{1}{\delta^{m+1}}\left[y_8+y_9^{'}\right]-Re\mu_e\frac{r}{\delta^{2m+m}}y_1y_8=0 \tag{23}$$

$$(m+1)\frac{r^{m+1}}{\delta^{m+1}}\lambda y_{10}+\frac{1}{Sc}y_{11}^{'}-r^2Sry_5^{'}-CrRe^2y_{10}=0 \tag{24}$$

Where;

$y_1^{'}=F^{'}=y_2$

$y_2^{'}=F^{''}=y_3$

$$y_3^{'}=F^{'''}=\frac{-c(n-1)\theta^{c(n-1)-2}\left[c(n-1)-1\right]y_2-c(n-1)\theta^{c(n-1)-1}\left[2y_3+4y_1\right]}{\theta^{c(n-1)}}$$
$$\frac{+2R_e\frac{r}{\delta^{m+1}}y_1y_2+Ha^2y_2-R_m\frac{Ha}{r\sqrt{\sigma\mu_o}}\frac{1}{\delta^{m+1}}\left[2y_8y_2+2y_1y_8-y_6y_1\right]}{\theta^{c(n-1)}}$$
$$\frac{+Re.R_m\frac{r^2\mu_e}{\rho}\frac{1}{\delta^{2m+2}}\left[y_8^2y_2+2y_1y_8y_9-2y_6y_8y_1\right]-(m+1)\frac{r^{m+1}}{\delta^{m+1}}\lambda y_2}{\theta^{c(n-1)}}-4y_2 \quad \textbf{(A)}$$

$y_4^{'}=\omega^{'}=y_5$

$$y_5^{'}=\omega^{''}=Pr\left[-(m+1)\frac{r^{m+1}}{\delta^{m+1}}\lambda y_4-\theta^{c(n-1)}\frac{Ec}{\delta^{m+1}}\left[4y_1^2+y_2^2\right]\right.$$
$$\left.-\frac{J}{\delta^{m+1}}y_1^2+2r\sqrt{\frac{\mu_e}{\rho}\frac{ReR_m}{Ha^2}}\frac{J}{\delta^{2m+2}}y_1^2y_8-\frac{r^2\mu_e}{\rho}\frac{ReR_m}{Ha^2}\frac{J}{\delta^{3m+3}}y_1^2y_8^2\right] \quad \textbf{(B)}$$

$y_6^{'}=\gamma^{'}=y_7$

$$y_7^{'}=\gamma^{''}=\left[-(m+1)\frac{r^{m+1}}{\delta^{2m+2}}\lambda y_6+Re\mu_e\frac{r}{\delta^{2m+m}}y_1y_6\right]Pr_{(m)}\delta^{m+1}-y_6 \quad \textbf{(C)}$$

$y_8^{'}=\varphi^{'}=y_9$

$$y_9^{'}=\phi^{''}=\left[-(m+1)\frac{r^{m+1}}{\delta^{2m+2}}\lambda y_8+Re\mu_e\frac{r}{\delta^{2m+m}}y_1y_8\right]Pr_{(m)}\delta^{m+1}-y_8 \quad \textbf{(D)}$$

$y_{10}^{'}=\phi^{'}=y_{11}$

$$y_{11}^{'}=Sc\left[r^2Sry_5^{'}+CrRe^2y_{10}-(m+1)\frac{r^{m+1}}{\delta^{m+1}}\lambda y_{10}\right] \quad \textbf{(E)}$$

In matrix form,

$$y=\begin{pmatrix}y_1\\y_2\\y_3\\y_4\\y_5\\y_6\\y_7\\y_8\\y_9\\y_{10}\\y_{11}\end{pmatrix}\Longrightarrow f=y^{'}=\begin{pmatrix}y_2\\y_3\\A\\y_5\\B\\y_7\\C\\y_9\\D\\y_{11}\\E\end{pmatrix}$$

Similarly, reducing the order of the dimensionless boundary conditions in equation 15 yields;

$$\begin{cases} \text{At the centre line;} \quad \theta = 0; \quad y_1(0) = 1, \quad y_2(0) = 0, \quad y_4(0) = \delta^{m+1}, \quad y_{10}(0) = 0 \\ \text{On the conduits wall;} \quad \theta = \alpha; \quad y_2(\alpha) = -\beta y_1(\alpha), \quad y_4(\alpha) = 0, \quad y_{10}(\alpha) = \delta^{m+1} \end{cases} \tag{25}$$

The BVP4C function in MATLAB implements the collocation technique, to determine the numerical solution of the first-order differential equations subject to the boundary conditions and the collocation conditions imposed in each sub-interval. In context to our study, the initial guess values provided to guide the solver on the optimum solution were obtained from the study on convergent conduit by [4]. According to [25], the BVP4C function estimates the error of the numerical solution on each sub-interval to satisfy the tolerance criteria and adapts an appropriate mesh. Further, reducing the step size of the adapted mesh increases the convergence of the method by ensuring the results tend to the exact solution.

3. Results and Discussion

In this section, the flow variables profiles i.e. velocity, temperature, species concentration and induced magnetic field in r and θ directions have been discussed. Similarly, various flow parameters are varied at a time and their impact on the flow variables determined.

3.1. Flow Profiles

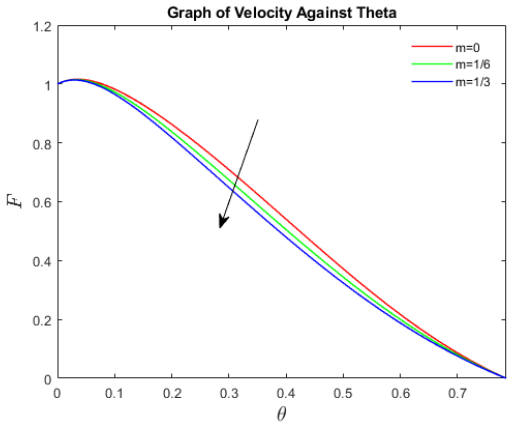

Fig. 2. Velocity profiles

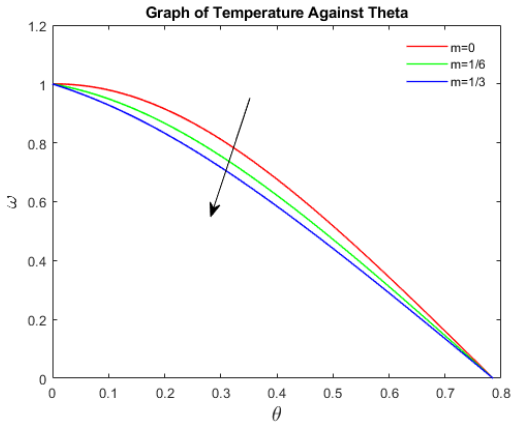

Fig. 3. Temperature profiles

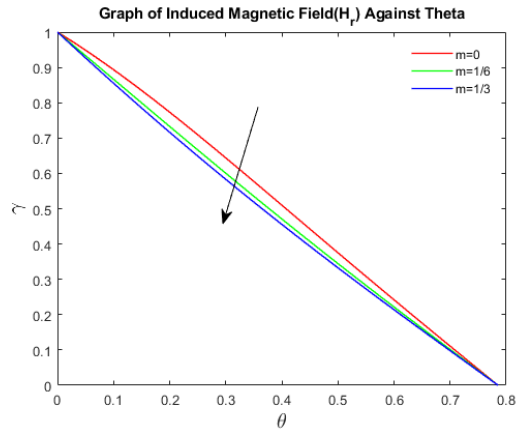

Fig. 4. Induced Magnetic Field profiles (H_r)

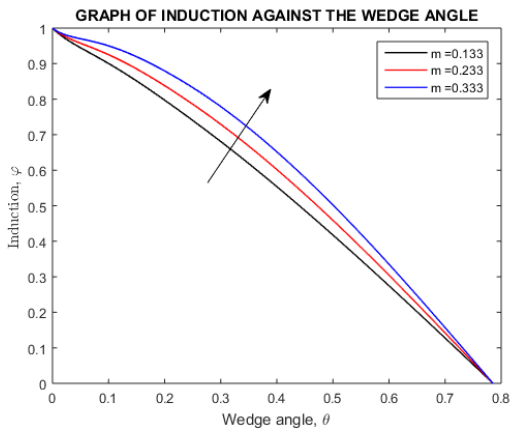

Fig. 5. Induced Magnetic Field profiles (H_θ)

The flow profiles are determined by taking different values of the arbitrary constant m which is related to the conduit's semi-angle as shown in the wedge angle parameter. In context with our study, the conduit's semi angle; $\alpha = [0, 45^\circ]$ which is equivalent to $[0, 0.7854^c]$ hence the arbitrary constant m is within the range $[0, \frac{1}{3}]$. Having the

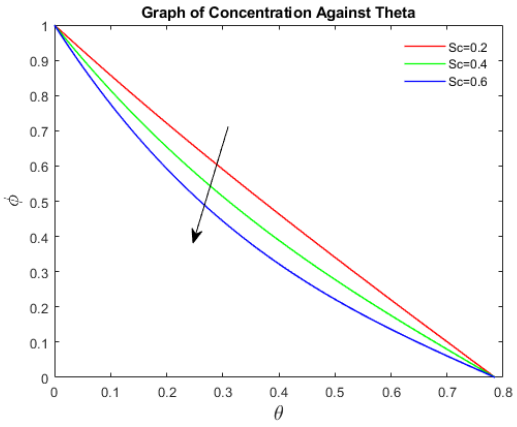

Fig. 6. Effect of varying Sc on concentration

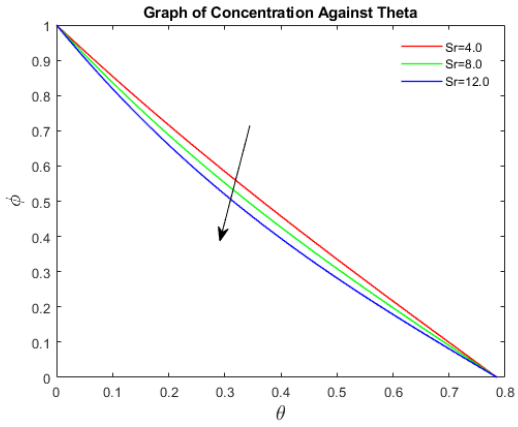

Fig. 7. Effect of Sr on the solute concentration

angle from the center-line to the conduit's wall as 45° is mainly to ensure a smooth flow transition for the fluid. This reduces the likelihood of turbulence, abrupt change in velocity and flow separation which can lead to pressure variation.

Fig. 2, Fig. 3, Fig. 4, and Fig. 5 shows the variation of velocity, temperature and induced magnetic field in r & θ directions respectively with the wedge angle for various values of m. The velocity, temperature and induced magnetic field in r & θ reduced with an increase in the conduit's angle. This implies that these flow variables are high at the center line and decrease towards the conduit's wall since the skin friction and viscous forces at the wall retard the fluid's motion. However, the internal resistance decreases towards the centreline hence a gradual increase in the fluid velocity. Similarly, as the fluid viscosity increases towards the conduit's wall, the fluid temperature decreases since temperature and viscosity are inversely proportional in liquids. Therefore, at the centreline of the conduit, there is a high interaction of the applied magnetic field and fluid velocity. This increases the induced electric current which in turn increases the induced magnetic field in both r and θ directions.

Fig. 6 depicts the effects of varying Schmidt number on the concentration profiles. The solute concentration decreases with an increase in the Schmidt number. An increase in Schmidt number implies that the kinematic viscosity (momentum diffusivity) is greater than the mass diffusivity. This implies that the velocity boundary layer is thicker than the concentration boundary layer. On that account, the mass transfer rate is reduced due to the thin concentration boundary layer. This reduces the diffusivity of the species in the flow region, which explains the reduction in species concentration with an increase in Schmidt number.

Fig. 7 displays the effect of the Soret parameter on the species concentration. The Soret parameter quantifies the effects of the temperature gradient on the concentration gradient of the species. An increase in the Soret parameter implies that the thermal diffusion coefficient is more significant which leads to the species separation effect due to the temperature gradient. On that note, the species move from the high temperature region (center-line) to the lower temperature region (conduit's wall). This implies that the species accumulate at the conduit's wall hence creating a high concentration gradient.

Primarily, the Soret parameter has a direct influence on the species concentration but indirectly affects the fluid velocity, temperature and induced magnetic field. In that regard, the species concentration gradient created by the increase in the Soret parameter affects the fluid velocity by generating buoyancy forces. The buoyancy forces are due to the density variation caused by the concentration difference leading to convective fluid motion (buoyancy-driven convection/natural convection).

Fig. 8 displays the effect of the chemical reaction parameter on the species concentration. The chemical reaction parameter Cr, provides an insight on the chemical reaction kinetics, viscous effects and the fluid's motion. The increase in chemical reaction parameter basically implies that the chemical kinetics and viscous effects predominates the convective fluid transport. Thus, with increased chemical reaction in the fluid flow, the species concentration reduces.

Fig. 9 depicts the effect of increasing the Prandtl number on the temperature. The fluid temperature increases with an increase in the Prandtl number Pr. An increase in the Prandtl number implies that the kinematic viscosity predominates the fluid thermal diffusivity. On that note, the reduction in the thermal diffusivity results to a decrease in the thermal boundary layer thickness hence reducing the fluid temperature.

Fig. 10 shows the variation of temperature with Eckert number. It is observed that an increase in Eckert number increases the fluid's temperature. An increase in Eckert's number implies that the heat dissipation in the fluid flow

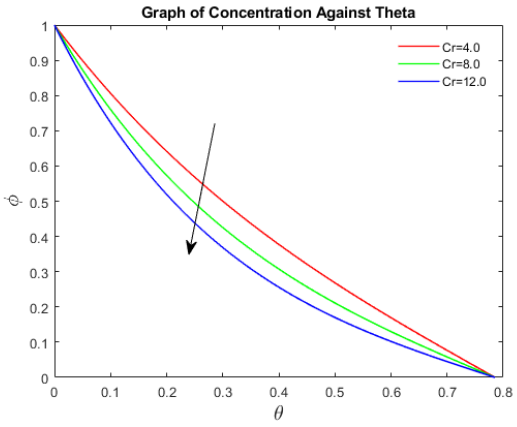

Fig. 8. Effect of Cr on the species concentration

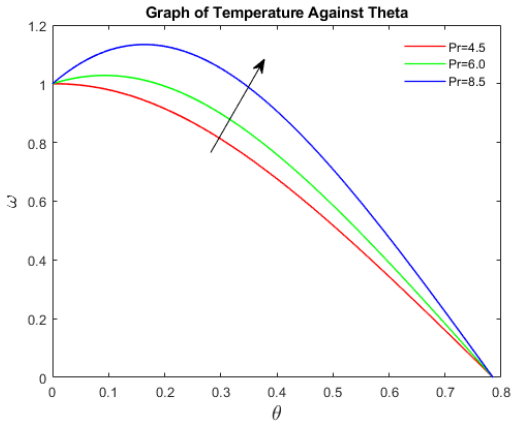

Fig. 9. Effect of varying Prandtl number on temperature

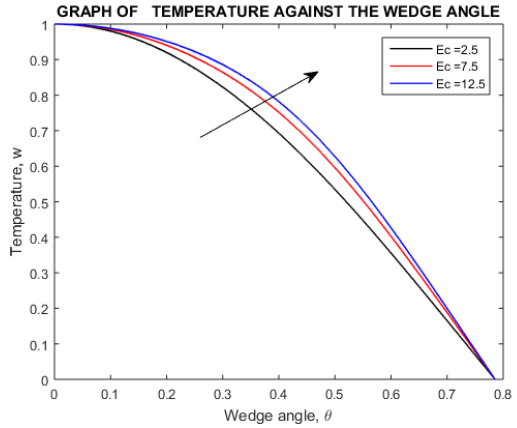

Fig. 10. Effect of varying Ec on Temperature

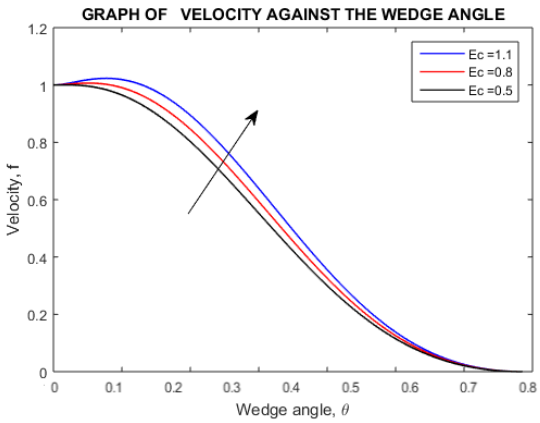

Fig. 11. Effect of varying Ec on velocity

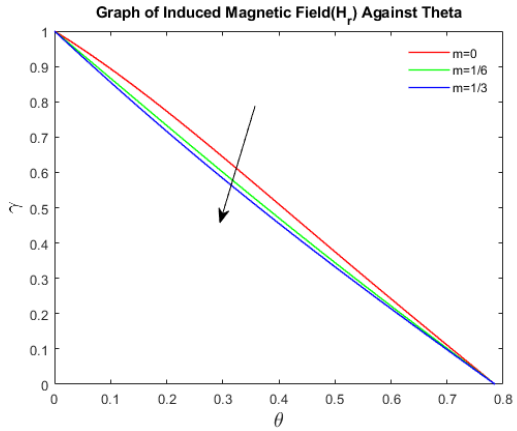

Fig. 12. Effect of varying Ec on (H_r)

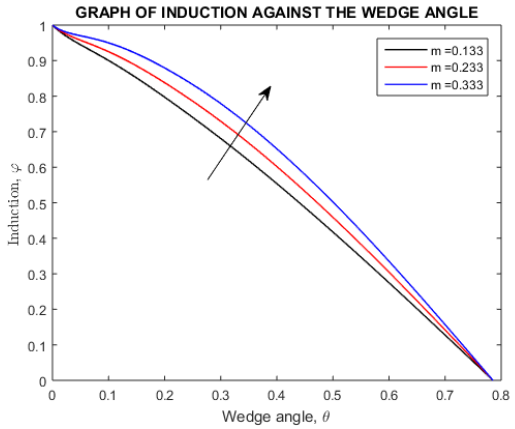

Fig. 13. Effect of varying Ec on (H_θ)

increases. Therefore, the increase in heat dissipation increases the fluid's temperature.

Fig. 11 shows the variation of velocity with Eckert number. The fluid velocity increases with an increase in Eckert number. The increase in Eckert number leads to an increase in temperature which implies that viscosity in the fluid flow decreases. Therefore, with decrease in viscosity, the fluid's velocity increases.

Fig. 12 and Fig. 13 shows the variation of induced magnetic field H_r and H_θ with Eckert number. The induced magnetic field in both r and θ direction increases with increase in Eckert number. An increase in Eckert's number increases the fluid's velocity. This increases the interaction between the applied magnetic field and the fluid's velocity.

This increases the induced magnetic field in r and θ direction.

Table 1. Skin friction coefficient values on variation of the flow parameters i.e. Eckerts number, Schmidt number, Chemical reaction parameter and the Prandtl number.

Skin friction coefficient	Eckert Number	Schmidt Number	Chemical reaction Parameter	Prandtl Number
1.88036	**4**	0.8	2	1.8
1.86224	**6**	0.8	2	1.8
1.84412	**8**	0.8	2	1.8
0.09456	5	**0.2**	2	1.8
0.11268	5	**0.4**	2	1.8
0.1308	5	**0.6**	2	1.8
0.1559	5	0.8	**4**	1.8
0.28990	5	0.8	**8**	1.8
0.4239	5	0.8	**12**	1.8
1.559	5	0.8	2	**4.5**
1.1730	5	0.8	2	**6**
1.3262	5	0.8	2	**8.5**

Table 1 shows the effect of varying the Eckert number, Schmidt number, chemical reaction parameter and Prandtl number on the skin friction coefficient. The skin friction coefficient is a quantity of practical interest which is proportional to $F^{'}(\theta)$. It depicts the highest frictional force existing between the conduit's wall and the fluid in motion.
The skin friction coefficient decreases with an increase in the Eckerts number. This is due to the increased heat dissipation in the fluid flow which in turn increases the fluid temperature. The increase in fluid temperature reduces the viscous and friction forces hence decreasing the skin friction coefficient.
On the other hand, the skin friction coefficient increases with an increase in the chemical reaction parameter, Schmidt number and Prandtl number. This implies that the viscous forces predominate, thus the formation of the boundary layer extends extremely into the flow region. This explains the increase in the skin friction coefficient.

Table 2. Nusselt number values on the variation of the flow parameters i.e. Eckerts number, Schmidt number, Chemical reaction parameter and the Prandtl number.

Nusselt number	Eckert Number	Schmidt Number	Chemical reaction Parameter	Prandtl Number
4.18835	**4**	0.1	3	1.8
4.55152	**6**	0.1	3	1.8
4.91469	**8**	0.1	3	1.8
4.0682	4	**0.2**	3	1.8
4.0562	4	**0.4**	3	1.8
4.0422	4	**0.6**	3	1.8
5.0211	4	0.1	**4**	1.8
4.9991	4	0.1	**8**	1.8
4.9871	4	0.1	**12**	1.8
5.82655	4	0.1	3	**4.5**
4.77089	4	0.1	3	**6**
4.18835	4	0.1	3	**8.5**

From Table 2 the Nusselt number provides an insight into the rates of heat transfer due to convection and conduction. In the study, the Nusselt number increases with an increase in the Eckerts number. This implies that the rate of heat transfer by convection predominates the rate of heat transfer due to conduction at the conduit's wall. This is due to the increase in fluid temperature which results from the internal heat generation.
Further, an increase in the Prandtl number, chemical reaction parameter and Schmidt number leads to a decrease in the Nusselt number. This implies that the rate of heat transfer by conduction predominates convectional heat transfer. This is because with the increase in the Prandtl number, chemical reaction parameter and Schmidt number, the fluid viscosity increases hence the fluid temperature decreases. Thus there is less heat transfer by convection in the fluid flow. This implies more thermal energy is lost at the conduit's wall through conduction.

4. Conclusion

In conclusion, the study examined heat and mass transfer in a non-Newtonian, electrically conducting fluid flow in a convergent conduit taking into account joule heating, viscous dissipation, Soret effects, chemical reactions and

variable magnetic field. The results depict that the concentration decreases with an increase in the Chemical reaction parameter, Soret parameter and Schmidt number. Further, temperature, velocity and induced magnetic field in r and θ directions increased with an increase in the Eckerts number.
This has notable application in fluid flow through the convergent conduit subsequent to the Pelton turbines. On that note, reducing the radius of the conduit will increase the Reynolds number which implies that the inertia forces increase thus the fluid velocity increases. Similarly, the heat loss at the conduit's wall can be minimized by using appropriate insulators at the wall hence maximizing the rate of heat transfer by convection which consequently increases the fluid velocity. Further, increasing the rate of change in magnetic flux B will increase the induced current which consequently increases the joule heating process hence minimizing the fluid's viscosity and the friction force that exists between the fluid in motion and the wall surface. On this account, the fluid's velocity will increase.

Availability of Data

The data used to support the findings of this study are included within the article.

Conflicts of Interest

The author declares that there are no conflicts of interest.

Acknowledgements

The author(s) would like to thank Jomo Kenyatta University of Agriculture and Technology for support in this project.

References

[1] G.B. Jeffery, “On the steady rotation of a solid of revolution in a viscous fluid," Proceedings of the London Mathematical Society, vol. 2, pp. 327-338, 1915.
[2] G. Hamel, “Spiral movements of viscous liquids," Jahresbericht der deutschen mathematiker-vereinigung, vol. 25, pp. 34-60, 1917.
[3] M. Asadullah and Khan, Umar and Ahmed, Naveed and Mohyud-Din, Syed Tauseef and others, "Analytical and numerical investigation of thermal radiation effects on flow of viscous incompressible fluid with stretchable convergent/divergent channels," Journal of Molecular Liquids, Elsevier, vol. 224, pp. 768-775, (2016)
[4] J. Nagler “Jeffery-Hamel flow of non-Newtonian fluid with nonlinear viscosity and wall friction,"Applied Mathematics and Mechanics, vol. 38, no. 6, pp. 319-340, 2017.
[5] M. Dhanalakshmi and Jayarami Reddy, K and Ramakrishna, K, "Chemical reaction and soret effects on MHD free convection flow past a vertical porous plate with heat generation," International Journal of ChemTech Research, vol. 9, no. 4, pp. 587-597, 2016.
[6] A. Hussanan and Salleh, Mohd Z and Khan, Ilyas and Tahar, Razman M and Ismail, Zulkhibri, "Soret effects on unsteady magnetohydrodynamic mixedconvection heat-and-mass-transfer flow in a porous medium with Newtonian heating," Maejo International Journal of Science & Technology, vol. 9, no. 2, 2015.
[7] E.R. Onyango, M. Kinyanjui, and S.M. Uppal, “Unsteady Jeffrey-Hamel Flow in the Presence of Oblique Magnetic Field with Suction and Injection," Applied and Computational Mathematics, vol. 9, no. 1, pp. 1-13, 2020.
[8] A.T Akinshilo, A. Ilegbusi, H.M. Ali, and A.J. Surajo, “Heat transfer analysis of nanofluid flow with porous medium through Jeffery Hamel diverging/converging channel,"Journal of Applied and Computational Mechanics, vol. 3, no. 6, pp. 433-444, 2020.
[9] K. Shukla and Shubham Kumar Dube, ”Numerical simulation of changes in Soret-Dufour number, Radiation, chemical reaction and viscous dissipation on instead MHD flow past an inclined porous plate embedded in porous medium with heat generation or absorption,” International Journal of Advances in Applied Mathematics and Mechanics, vol. 10, pp. 1-16, 2022.
[10] N.C Wawira, and Kinyanjui, Mathew and Giterere, Kang’ethe, "Hydromagnetic non-Newtonian fluid flow in a convergent conduit," Journal of Applied Mathematics, Hindawi, vol. 2022, pp. 1-16, 2022.
[11] Liberty Ebiwareme, and Kubugha Wilcox Bunonyo, “Application of Approximation Technique for the Effects of Chemical Reaction and Radiation Absorption of MHD Fluid flowing past an inclined porous plate in the presence

of inclined magnetic field," International Journal of Advances in Applied Mathematics and Mechanics, vol. 11, no. 1, pp. 1-12, 2023.

[12] L. Ali, B.Ali, X. Liu, T. Iqbal, R.M. Zulqarnain, and J. Muhammad, "A comparative study of unsteady MHD Falkner–Skan wedge flow for non-Newtonian nanofluids considering thermal radiation and activation energy," *Chinese Journal of Physics,* vol. 77, pp. 1625-1638, (2022).

[13] I.S Nima, S.O. Ferdows, M. Shamshuddin, M.D. Alsenafi, A. Abdulaziz, and A. Nakayama, "Melting effect on non-Newtonian fluid flow in gyrotactic microorganism saturated non-darcy porous media with variable fluid properties," Applied Nanoscience, vol. 10, no. 10, pp. 3911-3924, 2020.

[14] G.R. Rajput, M.D. Shamshuddin, Salawu, and O. Sulyman, "Thermosolutal convective non-Newtonian radiative Casson fluid transport over a vertical plate propagated by Arrhenius kinetics with heat source/sink," *Heat Transfer,* vol. 50, no. 3, pp. 2829-2848, 2021.

[15] V. Ojiambo, M. Kinyanjui, and M. Kimathi, A study of two-phase Jeffery Hamel flow in a geothermal pipe, IJAAMM, 2018.

[16] F.O. Ochieng, M.N. Kinyanjui, and M. Kimathi, "Hydromagnetic Jeffery-Hamel Unsteady Flow of a Dissipative Non-Newtonian Fluid with Nonlinear Viscosity and Skin Friction," Doctoral dissertation, JKUAT-PAUSTI, 2018.

[17] A.C Das, Nasa Qazi Novera, Tansue, and M.D.Alam Sarwar, "Analysis of magnetohydrodynamic jeffery-hamel flow in a convergent-divergent channel using Cu-water nanofluid" Journal of Engineering Science, vol. 12, no. 2, pp. 79-92, 2021.

[18] A. Liagat, A. Bagh, L. Xiaomin, A. Shehzad and S. Murad Ali, "Analysis of bio-convective MHD Blasius and Sakiadis flow with Cattaneo-Christov heat flux model and chemical reaction." Chinese Journal of Physics, vol. 77, 1963-1975, 2022.

[19] M. Faraday, "On the forms and states assumed by fluids in contact with vibrating elastic surfaces," *Phil. Trans. R. Soc. Lond..,* vol. 121, pp. 815-830, 1831.

[20] F. W. Sear, "Faraday's law and Ampere's law," *American Journal of Physics,* vol. 6, no .31, pp. 439-443, 1963.

[21] A. Salih, "Conservation equations of fluid dynamics," Department of Aerospace Engineering Indian Institute of Space Science and Technology, Thiruvananthapuram, 2011.

[22] Mwamba Nictor, O A. Jeconia and A. K Otieno "Effects of Thermal Radiation and Chemical Reaction on Hydromagnetic Fluid Flow in a Cylindrical Collapsible Tube with an Obstacle" International Journal of Mathematics and Mathematical Sciences vol. 2023, no. 1, pp. 1-13, 2023.

[23] M.D. Alam, and M.A.H. Khan, "Critical behaviour of the MHD flow in convergent-divergent channels," *Journal of Naval Architecture and Marine Engineering,* vol. 7, no. 2, pp. 83–93, 2010.

[24] M.Rahman, "New approach to partial differential approximants," 2004.

[25] L. F. Shampine, J. Kierzenka, and M.W. Reichelt, "Solving boundary value problems for ordinary differential equations in MATLAB with bvp4c," Tutorial notes, pp.1-27, 2000.